applied sciences

Article

Optimization of a Permanent Magnet Synchronous Motor for e-Mobility Using Metamodels

Se-eun Kim and Yong-min You *

Department of Automotive Engineering, Honam University, 112 Honamdae-gil, Gwangsan-gu, Gwangju 62399, Korea; lpm3388@naver.com
* Correspondence: ym.you@honam.ac.kr; Tel.:+82-62-940-5499

Abstract: Permanent magnet synchronous motors (PMSMs) with rectangular coils in hairpin windings exhibit improved fill factor and reduced end turn of the coils, which in turn improve the efficiency and power density of PMSMs, making them ideal for e-mobility applications. Herein, the shape of a PMSM was optimized for torque ripple reduction using metamodels to improve the noise and vibrational performance of the motor. The objective function of the optimal design aimed to minimize the torque ripple, and the average torque and efficiency were set as constraints. The notch width and depth and barrier length were selected as the design variables to satisfy the objective function and constraints. Using the optimal Latin hypercube design technique, 27 experimental points were selected, and a finite element analysis (FEA) was performed for each point. Furthermore, a function approximation was performed using six metamodels, and the best metamodel was selected using the root mean square error test. Moreover, the optimization was performed by combining the best metamodels for each variable with a sequential two-point diagonal quadratic approximation optimization algorithm. The torque ripple was improved by approximately 1.63% compared with the initial model, whereas the constraint values remained constant. Finally, an FEA was performed on the optimal point, and the FEA results matched with those of the optimal method.

Keywords: optimization; PMSM; hairpin winding; e-Mobility; metamodel

check for updates

Citation: Kim, S.-e.; You, Y.-m. Optimization of a Permanent Magnet Synchronous Motor for e-Mobility Using Metamodels. *Appl. Sci.* **2022**, *12*, 1625. https://doi.org/10.3390/app12031625

Academic Editor: Mariusz Jagiela

Received: 14 January 2022
Accepted: 31 January 2022
Published: 3 February 2022

1. Introduction

Vehicular pollution has considerably increased in recent years due to urbanization and has become one of the major contributors to environmental pollution. To overcome this problem, electro mobility or e-mobility, which offers an eco-friendly means of transportation, especially in the urban areas, has been gaining considerable traction [1]. The e-mobility industry comprises a wide variety of vehicles, ranging from electric kickboards and Segways, to electric scooters and cars [2]. The key components of any electric vehicle include a motor, battery, and power converter [3]. Among these key components, a traction motor capable of delivering high output at high efficiency was considered in this study.

Permanent magnet synchronous motors (PMSMs) have been widely used in a variety of industries (such as appliances, industrial tools, and driving motors for electric vehicles) because of their excellent efficiency, torque density, and low maintenance [4–7]. PMSMs with rectangular coils in hairpin winding arrangements can reduce the space factor by reducing the unnecessary space in the slots when compared with those with round coils [8]. In addition, since the copper loss is reduced by reducing the end turn of the coils, the efficiency and output density of the motor can be significantly improved [9].

However, torque ripple in PMSM causes vibrations and noise, and there are several studies being conducted to reduce this [10]. There are various methods for reducing the torque ripple as reported in the contemporary literature, such as changing the shape of the stator, rotor, and shoe, and applying a skew and notch. In [11], the torque ripple was minimized by designing a cavity on the rotor. In [12], the shape of the barrier of the rotor was optimized using a response surface methodology, which is an experimental design method, and a wedge skew was applied to the shoe of the stator to reduce the torque ripple. In another study, the torque ripple was reduced by applying a non-uniform air gap and rotor hole [13]. In [10], the torque ripple was reduced by applying a notch to the rotor. In studies in which the torque ripple was reduced by applying a notch, circular notches were predominantly used [14]. In this study, an elliptical-shaped notch was applied to determine the torque characteristics of a PMSM based on the width and depth of a notch. In addition, the barrier length of the rotor was set as a design variable to improve the performance of the motor.

Two methods have been considered as general optimal design methods. In the first method, an approximation function is generated using metamodeling processes based on the design of experiments (DoE) results. Then, the approximated function is combined with an optimal algorithm to determine the optimal values. The second method connects the analysis model and optimal algorithm directly and iteratively analyzes the values until the optimal design values are found. In the former method, the accuracy of the metamodel significantly affects the optimal design results. In most extant studies, the experiments were conducted to approximate the relationship between the input and output variables using only one metamodel technique [15,16]. However, due to the existence of a variety of metamodeling techniques, it is important to apply the most appropriate one for each design problem. Therefore, in this study, the relationship between the input and output variables is expressed as an approximation function by applying six metamodel techniques for each objective function and constraint. In addition, to compensate for the low accuracy, which is a disadvantage of the optimal design method using metamodels, the best metamodel technique with the lowest error as ascertained by the root mean square error (RMSE) test was applied.

The differences between this study and previous studies are as follows. First, in previous studies, the reduction in the torque ripple based on the width and depth of the notch was studied by applying an elliptical-shaped notch, instead of a circular notch, to the stator teeth. In addition, the shape of the flux barrier was set as a design variable to compensate for the decrease in the average torque and efficiency of the motor when applying the notch. Second, in most previous studies, only one metamodeling technique was applied to approximate the optimization function. However, in this study, the function approximation was performed by applying six metamodeling techniques for each objective function and constraint. In addition, the optimal design was performed by selecting the best metamodel method obtained using the RMSE test.

In this study, the shape optimization of a PMSM for e-mobility was performed. The objective function of the optimal design aimed to minimize the torque ripple, wherein the average torque and efficiency were set as constraints. Three design variables were selected to satisfy the objective function and the constraints. There are various methods such as full factorial, central composite design, and Plackett–Burman for the sampling strategy for DoE [17]. If there is the existence of nonlinearity in the relation between design variables and output variables, the prediction accuracy is better when the optimal Latin hypercube design (OLHD) technique is used [18]. Additionally, using the OLHD technique, 27 experimental points were determined for the DoE. The DoE for the selected experimental points were obtained using a finite element analysis (FEA) method. The correlations between the design variables and responses were investigated by applying a screening technique with the DoE results. Metamodels of the objective function and constraints were established using the DoE results, and the metamodels with the highest accuracy were selected using accuracy evaluations. These metamodels were combined with the sequential two-point diagonal quadratic approximate optimization (STDQAO) algorithm to find an optimal solution. Finally, the adequacy of the optimal design for the optimal point was verified using FEA.

2. Torque Ripple

Torque ripple is caused by a change in the magnetic energy between the permanent magnets of the rotor and slots of the stator of a PMSM [19]. When the magnetic energy changes depending on the relative position of the magnetic pole and slot in a rotating motor, a reluctance torque is generated by the slot structure; this results in a torque ripple, which causes noise and vibrations in traction motors. As such, the torque ripples must be minimized. Moreover, traction motors used in electric vehicles should have torque ripple values of < 10% [20].

2.1. Initial Model of the PMSM

The shape of the initial model of a PMSM with output power of 8 kW is shown in Figure 1. The motor has 6 poles and 36 slots and is an interior-type PMSM, in which the permanent magnet is located inside the rotor core. Table 1 lists the specifications of the initial model of the PMSM. As shown in Figure 1, the N42UH grade NdFeB permanent magnets are arranged in a V-shape topology, and 35PN440 grade electrical steels are used for the stator and rotor core. In addition, a hairpin winding arrangement with a rectangular cross section is used to improve the fill factor of the coil.

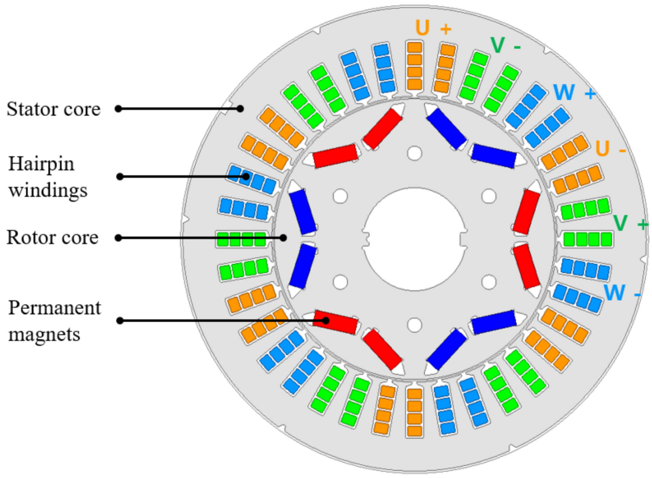

Figure 1. Shape of the initial model of the permanent magnet synchronous motor (PMSM).

Table 1. Specifications of the initial model of the PMSM.

Parameters	Unit	Value
Rated output power	kW	8
Rated torque	N·m	25
Rated speed	rpm	3000
Electrical steel	-	35PN440 (POSCO)
Permanent magnet	-	N42SH
Continuous current	A_{rms}	150
Current phase angle	°	40
Copper conductor size	mm	3*4
No. of coil turns	turns	4
No. of poles and slots	ea	6/36
Outer diameter of stator	mm	135
Air-gap	mm	0.75
Lamination	mm	50

2.2. Analysis Result of the Torque Ripple

The torque waveform of the initial model, as shown in Figure 2, was analyzed using Ansys Maxwell, which is electromagnetic field analysis software. The difference between the maximum and minimum value of the torque was 1.686 N·m, and the average torque value was 25.296 N·m. Using Equation (1), the torque ripple value of the initial model was calculated as 6.664% [13].

$$T_{ripple} = \frac{T_{max} - T_{min}}{T_{avg}} \times 100\% \tag{1}$$

where T_{max} is the maximum torque, T_{min} is the minimum torque, and T_{avg} is the average torque.

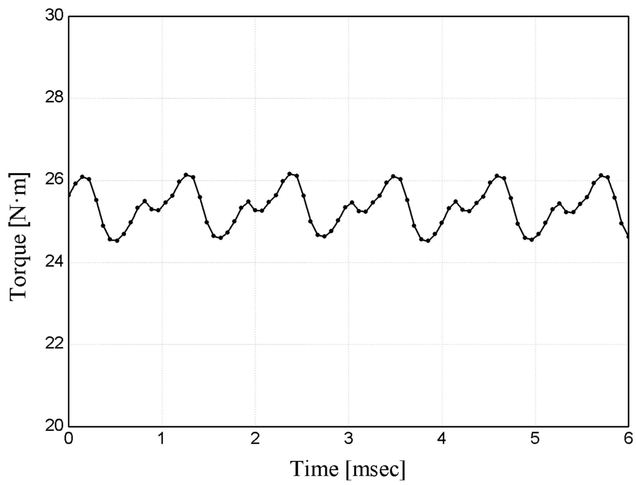

Figure 2. Torque waveform of the initial model.

3. Design Optimization

3.1. Optimization Process

Figure 3 shows a flowchart of the design optimization of a PMSM. The formulation of the design problem is defined by Equations (2)–(4). The objective function was to minimize the torque ripple, and the average torque and efficiency were set as constraints. To maintain the same performance of the initial model even in the case of reduced torque ripple values, the efficiency and average torque values were set as the lower limits of the constraints. The design variables to satisfy the objective function and constraints are shown in Figure 4, and the limits of these design variables are listed in Table 2. The upper limit of the stator notch width (X1) and stator notch depth (X2) were set based on the mechanical stiffness. The limits of the barrier length (X3) are set according to the magnetic flux flow.

Table 2. Range of design variables.

Design Variables	Unit	Initial	Lower	Upper	Considerations
Stator Notch width (X1)	mm	0	0	2.8	Mechanical stiffness
Stator Notch depth (X2)	mm	0	0	0.7	Mechanical stiffness
Barrier length (X3)	mm	0	0	1	Magnetic flux flow

Objective function

$$\text{Minimize the torque ripple} \tag{2}$$

Constraints

$$\text{Average torque} \geq 25.296\ \text{N·m} \tag{3}$$

$$\text{Efficiency} \geq 90.108\% \tag{4}$$

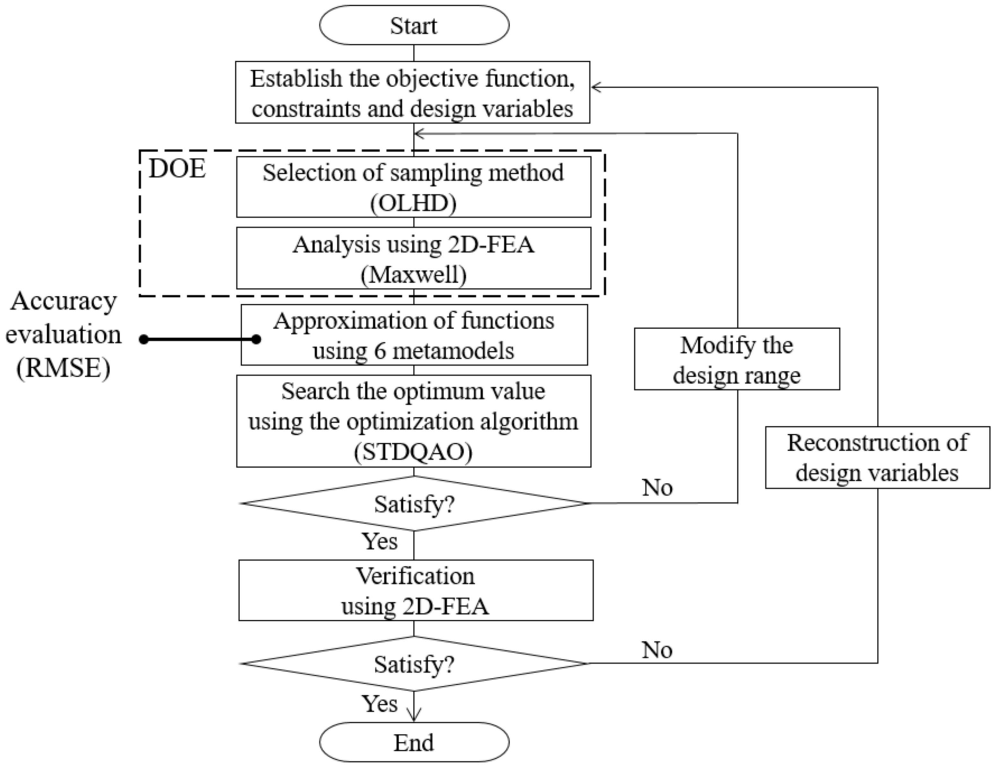

Figure 3. Flowchart of the design optimization of a PMSM.

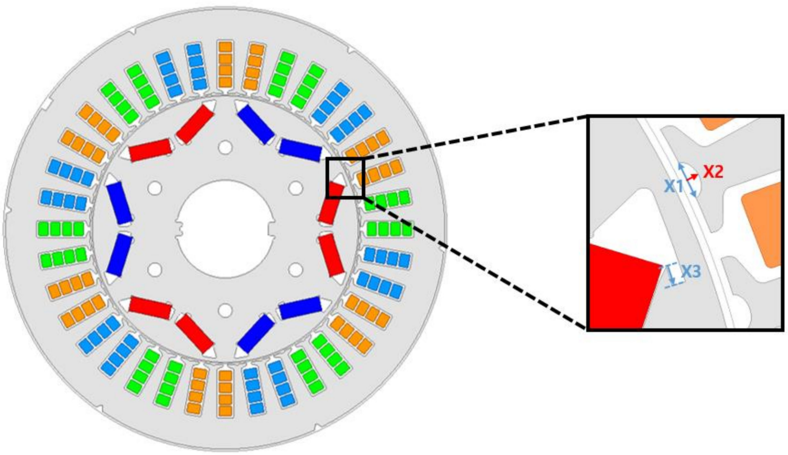

Figure 4. Optimal design variables.

3.2. Design of Experiment

To improve the accuracy of the metamodel, the design points should be evenly distributed within the design domain [21]. In this study, the DoE was performed using the OLHD sampling technique, which provides excellent space filling with limited sampling points [22]. To evaluate the accuracy of the metamodel, the number of experiments and test points were set as 27 and 3, respectively, using Equations (5) and (6) [23]. Additionally, FEA was performed for each sampling point selected by the OLHD sampling technique.

$$nEXP > min\left[\frac{(nDV+1)\times(nDV+2)}{2},\ 10\times nDV\right] + (5\times nDV) \tag{5}$$

where $nEXP$ is the number of DoEs, and nDV is the number of design variables.

Using Equation (5), the minimum number of DoEs obtained was 25 because the number of design variables was 3. Moreover, the number of DoEs was set as 27, which is a multiple of the number of design variables.

$$nEXP\_ts > min[nEXP \times 10\%,\ 10 \times nDv] \tag{6}$$

where $nEXP\_ts$ refers to the number of test points.

3.3. Sensitivity Analysis

Sensitivity analysis was performed based on the aforementioned 27 experiments to determine the design variables that affect the output variables [24]. Figure 5 shows that the torque ripple of the objective function is the most affected by the barrier length (X3). In addition, it was confirmed that the average torque and efficiency were mainly affected by the notch width (X1) and notch depth (X2).

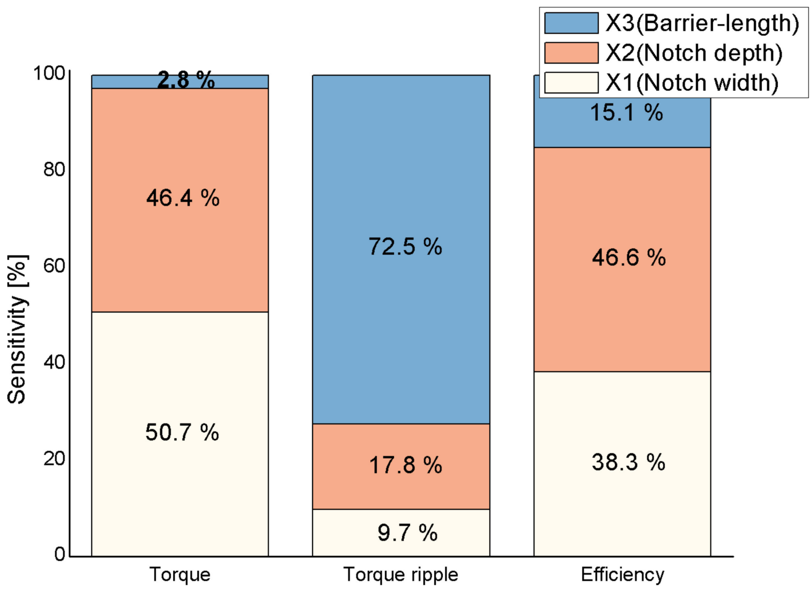

Figure 5. Sensitivity analysis using the screening technique.

3.4. Metamodeling

Using the optimal design program called PIAnO, the correlations between the input and output variables were mathematically approximated [25]. Six metamodels were established for each output variable based on the DoE results. The ensemble of decision trees (EDT) is a regression model capable of dealing with large amounts of data [23]. The Kriging model, which is an interpolation model, passes exactly through the experimental points and can form complex models with a limited amount of data [16]. It is also possible to analyze prediction uncertainty using this model [26]. The multi-layer perception (MLP) model, comprising hidden and output layers, minimizes the error function using weights and biases [27]. The polynomial regression (PR) model, which uses the regression equation, can reduce errors and improve prediction performance [28]. Finally, the radial basis function (RBF) model can approximate the underlying model using the training dataset, and it can also generate a regression (Reg.) or an interpolation (Int.) model [29].

Optimal designs by approximation functions using metamodels suffer from the problem of low accuracy. In this study, this limitation was compensated by applying six metamodel techniques to the objective function and constraints. In addition, the RMSE test was conducted to evaluate the prediction performance of the metamodels. The value of the RMSE test was obtained using Equation (7), and the results of the RMSE test corresponding to each output variable for all six metamodels are summarized in Table 3 [30]. For each output variable, the metamodel with the lowest RMSE test value was selected. As can be seen from Table 3, the Kriging metamodel is the most suitable for the torque ripple variable, and the PR (Forward Step.) is the most suitable for both the average torque and efficiency variables.

$$RMSE = \frac{1}{n_{test}}[y(x_i) - \hat{y}(x_i)]^2 \tag{7}$$

where n_{test} is the number of experimental points used to evaluate the metamodel, and $y(x_i)$ and $\hat{y}(x_i)$ are the values of the actual function and approximate function, respectively.

Table 3. RMSE test results of the metamodels for different output variables.

Metamodel	RMSE Test Value		
	Torque Ripple	**Average Torque**	**Efficiency**
EDT (Hybrid)	0.861980	0.108295	0.029970
Kriging	0.444338	0.081922	0.027080
MLP	0.653252	0.063183	2.723662
PR (Forward Step.)	0.695273	0.029480	0.012375
RBF (Int.)	1.381964	0.062220	0.019989
RBF (Reg.)	0.778125	0.092219	0.241133

3.5. Optimization Results

The CPU of the workstation used to derive the optimal design was an Intel Xeon W-2235 processor with 64 GB RAM. The best metamodels of the three output variables as selected by the RMSE test were combined with hybrid metaheuristic algorithm (HMA) and STDQAO, respectively. HMA is a kind of evolutionary algorithm, and STDQAO is a kind of gradient-based optimization algorithm. In general, evolutionary algorithms show better optimization results than gradient-based algorithms. However, in the case of this optimization, when STDQAO was applied, better results were shown than when HMA was applied, as shown in Table 4. The torque ripple of the optimal model was improved by approximately 1.63% compared with that of the initial model. In addition, it was confirmed that the average torque and efficiency of the optimal model were similar to those of the initial model. Figure 6 shows the torque waveforms of the initial and optimal models. The optimal design based on the metamodel generated predictive values of the design variables; therefore, an FEA was performed in this study to verify the adequacy of the design. As observed from the data presented in Table 4, the optimal design and FEA values of the variables are almost identical.

Table 4. Optimization results.

Items		Unit	Initial	Optimal (HMA)		Optimal (STDQAO)	
				Predicted	**FEA**	**Predicted**	**FEA**
Design variables	Notch width (X1)	mm	1.504	1.655		1.504	
	Notch depth (X2)	mm	0.398	0.420		0.398	
	Barrier length (X3)	mm	0.072	0.072		0.072	
Design results	Torque ripple	%	4.835	4.816	5.092	4.835	5.032
	Average torque	N·m	25.278	25.251	25.253	25.278	25.284
	Efficiency	%	90.118	90.111	90.113	90.118	90.120

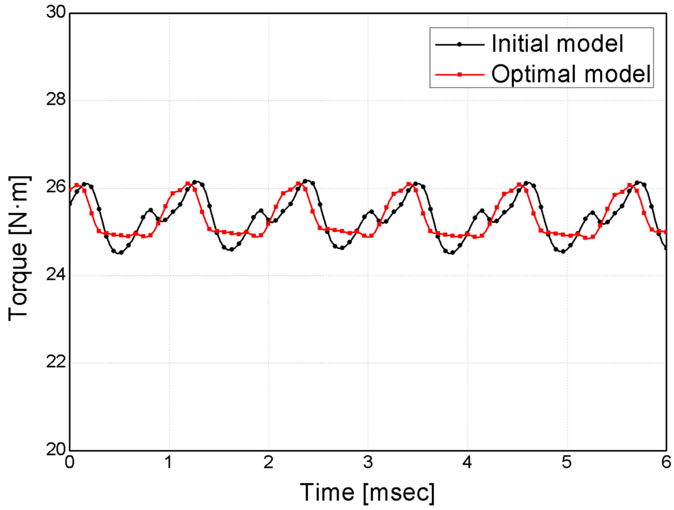

Figure 6. Torque waveforms of the initial and optimal models.

3.6. Mechanical Stress Analysis

When the structure of the rotor changes, it is accompanied by a change in the mechanical stress. Therefore, a mechanical stress analysis was performed on the rotor of the optimal model using Ansys Mechanical. Table 5 shows the material properties of the rotor core and the permanent magnet constituting the rotor. Since the maximum mechanical stress at the rated speed was 3.763 MPa, as shown in Figure 7, it was found to be very safe when compared with the tensile yield strength in Table 5.

Table 5. Material properties for mechanical stress analysis.

Items	Unit	Rotor Core (35PN440)	Permanent Magnet (N42SH)
Density	kg/m^3	7700	7400
Poisson's ratio	–	0.25	0.33
Young's modulus	GPa	195	152
Tensile yield strength	MPa	273	75

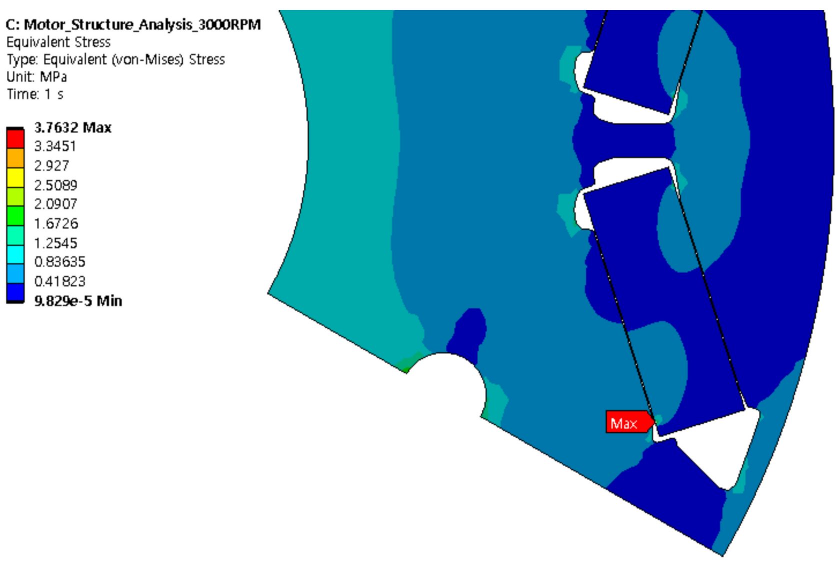

Figure 7. Mechanical stress analysis results.

3.7. Consideration

The number of electrical slots in the optimal design model was increased by incorporating notches in the stator teeth of the PMSM. The peak-to-peak value of cogging torque is inversely proportional to the least common multiple of poles and slots numbers [31]; this contributed toward a reduction in the cogging torque, and consequently, the torque ripple. The FEA results confirmed that the cogging torque of the optimal model was reduced by 33.3% compared with that of the initial model, as shown in Figure 8. To analyze the effects of the stator notch and flux barrier on the motor characteristics, an additional analysis was performed; the results of this analysis are summarized in Table 6. When only the notch was applied, the torque ripple reduced in the optimal model more than in the initial model, and the average torque and efficiency also reduced. The shape change of the flux barrier alone reduced the torque ripple, and it also increased the average torque and efficiency. However, the combined effect of both the notch and flux barrier confirmed that the torque ripple was reduced to its minimum value, whereas the average torque and efficiency values remained the same as those of the initial model. The magnetic flux flow and saturation of the magnetic flux density of the optimal model were similar to those of the initial model, as shown in Figures 9 and 10.

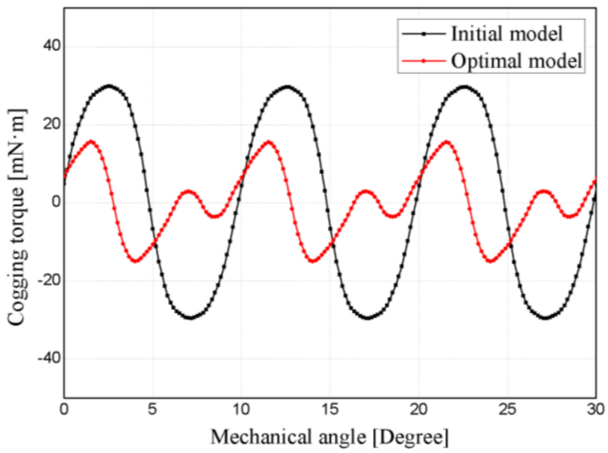

Figure 8. Cogging torque waveforms of the initial and optimal models.

Table 6. Analysis results of design variables for the notch and flux barrier.

Items		Unit	Initial	Notch	Flux Barrier	Optimal (FEA)
Design variables	Notch width (X1)	mm	0	1.504	0	1.504
	Notch depth (X2)	mm	0	0.398	0	0.398
	Barrier length (X3)	mm	0	0	0.072	0.072
Design results	Torque ripple	%	6.664	6.391	5.234	5.032
	Average torque	N·m	25.296	25.154	25.426	25.284
	Efficiency	%	90.108	90.074	90.153	90.120

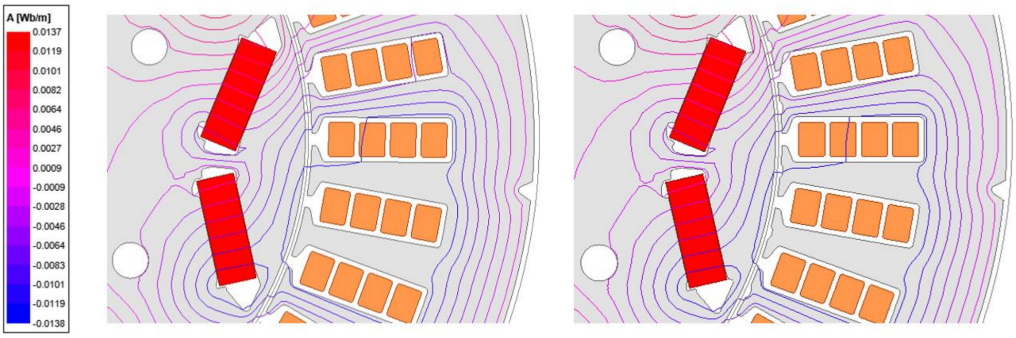

(a) (b)

Figure 9. Flux distribution at the load operation: (**a**) Initial model; (**b**) Optimal model.

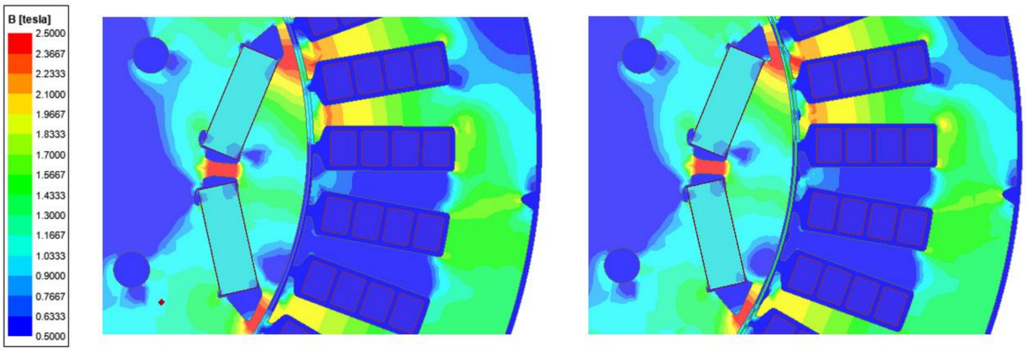

(a) (b)

Figure 10. Flux density distribution at the load operation: (**a**) Initial model; (**b**) Optimal model.

The optimal design results after applying both the best and worst metamodels were compared, as presented in Table 7. When the best metamodels were applied, the variation between the optimal model and FEA results was minimal. However, when the worst metamodels were applied, large errors occurred between them. In particular, the largest error occurred in the torque ripple. In addition, it was confirmed that the torque ripple of the best model was 5.032%, which is significantly better compared with 6.522% of the worst metamodel. Through additional analysis, it was found that the best metamodel exhibits higher accuracy and better performance than the worst metamodel. Therefore, after comparing the RMSE test results of the different metamodel techniques, the best metamodel with the highest accuracy was applied in this study and its validity was verified.

Table 7. Comparison of the optimal design results for the best and worst metamodels.

Items	Unit	Initial	Best Metamodel (STDQAO)	Best Metamodel (FEA)	Worst Metamodel (STDQAO)	Worst Metamodel (FEA)
Notch width (X1)	mm	0	1.504		1.457	
Notch depth (X2)	mm	0	0.398		0.308	
Barrier length (X3)	mm	0	0.072		0	
Torque ripple	%	6.664	4.835	5.032	4.529	6.522
Average torque	N·m	25.296	25.278	25.284	25.323	25.195
Efficiency	%	90.108	90.118	90.120	90.130	90.083

4. Conclusions

In this study, the shape optimization of a PMSM for e-mobility applications was performed using metamodels. The objective function was set to minimize the torque ripple, and the average torque and efficiency were set as constraints. The width and depth of the stator notch and barrier length were set as design variables to satisfy the objective function and constraints. Using the OLHD technique, 27 sampling points were selected, and an FEA was performed for each sampling point. In addition, a screening technique was used to determine the correlation between the input and output variables of the DoE. Six different metamodel techniques were applied, and the RMSE test was used to select the best metamodels for each of the three output variables. The optimal point was found by combining the best metamodels with the STDQAO algorithm. Finally, an FEA of the optimal point was performed to verify the optimal design. The optimal design results confirmed that the torque ripple was improved by approximately 1.63% compared with the initial model, while maintaining the average torque and efficiency of the initial model. Therefore, this study showed that the torque ripple, which is a key characteristic of the PMSM for e-mobility, can be effectively reduced by optimizing the core shape of the motor.

Author Contributions: Analysis, optimal design and writing, S.-e.K.; writing, writing—review and editing, Y.-m.Y. All authors have read and agreed to the published version of the manuscript.

Funding: This study was supported by research fund from Honam University, 2021 and Basic Science Research Program through the National Research Foundation of Korea (NRF) funded by the Ministry of Education (NRF-2021R1I1A3060525).

Institutional Review Board Statement: Not applicable.

Informed Consent Statement: Not applicable.

Data Availability Statement: The data presented in this study are available on request from the corresponding author.

Acknowledgments: The authors express gratitude to TMSOLUTIOS and PIDOTECH for their technical support.

Conflicts of Interest: The authors declare no conflict of interest.

References

1. Şengül, B.; Mostofi, H. Impacts of E-Micromobility on the Sustainability of Urban Transportation—A Systematic Review. *Appl. Sci.* **2021**, *11*, 5851. [CrossRef]
2. Abduljabbar, R.L.; Liyanage, S.; Dia, H. The Role of Micro-Mobility in Shaping Sustainable Cities: A Systematic Literature Review. *Transp. Res. Part D Transp. Environ.* **2021**, *92*, 102734. [CrossRef]
3. Van Mierlo, J.; Berecibar, M.; El Baghdadi, M.; De Cauwer, C.; Messagie, M.; Coosemans, T.; Jacobs, V.A.; Hegazy, O. Beyond the State of the Art of Electric Vehicles: A Fact-Based Paper of the Current and Prospective Electric Vehicle Technologies. *World Electr. Veh. J.* **2021**, *12*, 20. [CrossRef]
4. Lee, H.-K.; Bang, T.-K.; Lee, J.-I.; Woo, J.-H.; Shin, H.-S.; Yoon, I.-J.; Choi, J.-Y. Analytical Study and Comparison of Electromagnetic Characteristics of 8-Pole 9-Slot and 8-Pole 12-Slot Permanent Magnet Synchronous Machines Considering Rotor Eccentricity. *Electronics* **2021**, *10*, 2036. [CrossRef]
5. Kotin, D.; Ivanov, I.; Shtukkert, S. Modified Permanent Magnet Synchronous Generators for Using in Energy Supply System for Autonomous Consumer. *Energies* **2021**, *14*, 7196. [CrossRef]
6. Bouguenna, I.F.; Tahour, A.; Kennel, R.; Abdelrahem, M. Multiple-Vector Model Predictive Control with Fuzzy Logic for PMSM Electric Drive Systems. *Energies* **2021**, *14*, 1727. [CrossRef]
7. Lakhe, R.K.; Chaoui, H.; Alzayed, M.; Liu, S. Universal Control of Permanent Magnet Synchronous Motors with Uncertain Dynamics. *Actuators* **2021**, *10*, 49. [CrossRef]
8. Choi, M.; Choi, G. Modeling, Investigation, and Mitigation of AC Losses in IPM Machines with Hairpin Windings for EV Applications. *Energies* **2021**, *14*, 8034. [CrossRef]
9. Agamloh, E.; von Jouanne, A.; Yokochi, A. An Overview of Electric Machine Trends in Modern Electric Vehicles. *Machines* **2020**, *8*, 20. [CrossRef]
10. Hwang, M.-H.; Lee, H.-S.; Cha, H.-R. Analysis of Torque Ripple and Cogging Torque Reduction in Electric Vehicle Traction Platform Applying Rotor Notched Design. *Energies* **2018**, *11*, 3053. [CrossRef]

11. Lee, M.; Hwang, Y.; Nam, K. Torque Ripple Minimizing of Uniform Slot Machines with Delta Rotor via Subdomain Analysis. *Energies* **2021**, *14*, 7390. [CrossRef]
12. Jang, H.; Kim, H.; Liu, H.-C.; Lee, H.-J.; Lee, J. Investigation on the Torque Ripple Reduction Method of a Hybrid Electric Vehicle Motor. *Energies* **2021**, *14*, 1413. [CrossRef]
13. Lukman, G.F.; Ahn, J.-W. Torque Ripple Reduction of Switched Reluctance Motor with Non-Uniform Air-Gap and a Rotor Hole. *Machines* **2021**, *9*, 348. [CrossRef]
14. Park, Y.-W.; Ko, J.-S.; Kim, D.-K. Optimal Design of Step-Sloping Notches for Cogging Torque Minimization of Single-Phase BLDC Motors. *Energies* **2021**, *14*, 7104. [CrossRef]
15. Park, J.-C.; Park, S.-H.; Kim, J.-H.; Lee, S.-G.; Lee, G.-H.; Lim, M.-S. Diagnosis and Robust Design Optimization of SPMSM Considering Back EMF and Cogging Torque due to Static Eccentricity. *Energies* **2021**, *14*, 2900. [CrossRef]
16. Hoang, P.H.; Phan, H.N.; Nguyen, D.T.; Paolacci, F. Kriging Metamodel-Based Seismic Fragility Analysis of Single-Bent Reinforced Concrete Highway Bridges. *Buildings* **2021**, *11*, 238. [CrossRef]
17. Orosz, T.; Gadó, K.; Katona, M.; Rassõlkin, A. Automatic Tolerance Analysis of Permanent Magnet Machines with Encapsuled FEM Models Using Digital-Twin-Distiller. *Processes* **2021**, *9*, 2077. [CrossRef]
18. Choi, Y.; Song, D.; Yoon, S.; Koo, J. Comparison of Factorial and Latin Hypercube Sampling Designs for Meta-Models of Building Heating and Cooling Loads. *Energies* **2021**, *14*, 512. [CrossRef]
19. Akay, A.; Lefley, P. Torque Ripple Reduction Method in a Multiphase PM Machine for No-Fault and Open-Circuit Fault-Tolerant Conditions. *Energies* **2021**, *14*, 2615. [CrossRef]
20. Chau, K.T. *Electric Vehicle Machines and Drives: Design, Analysis and Application*, 1st ed.; Wiley-IEEE: Hoboken, NJ, USA, 2015; p. 243.
21. Butler, N.A. Optimal and orthogonal Latin hypercube designs for computer experiments. *Biometrika* **2001**, *88*, 847–857. [CrossRef]
22. Park, J.; Yoo, D.; Moon, J.; Yoon, J.; Park, J.; Lee, S.; Lee, D.; Kim, C. Reliability-Based Robust Design Optimization of Lithium-Ion Battery Cells for Maximizing the Energy Density by Increasing Reliability and Robustness. *Energies* **2021**, *14*, 6236. [CrossRef]
23. You, Y.-M. Optimal Design of PMSM Based on Automated Finite Element Analysis and Metamodeling. *Energies* **2019**, *12*, 4673. [CrossRef]
24. Hancu, G.; Orlandini, S.; Papp, L.A.; Modroiu, A.; Gotti, R.; Furlanetto, S. Application of Experimental Design Methodologies in the Enantioseparation of Pharmaceuticals by Capillary Electrophoresis: A Review. *Molecules* **2021**, *26*, 4681. [CrossRef]
25. Jeong, C.H.; Ko, M.K.; Lee, M.; Lee, S.H. CFD-Based Metamodeling of the Propagation Distribution of Styrene Spilled from a Ship. *Appl. Sci.* **2020**, *10*, 2109. [CrossRef]
26. Aissa, M.H.; Verstraete, T. Metamodel-Assisted Multidisciplinary Design Optimization of a Radial Compressor. *Int. J. Turbomach. Propuls. Power* **2019**, *4*, 35. [CrossRef]
27. Kontogiannis, D.; Bargiotas, D.; Daskalopulu, A.; Tsoukalas, L.H. A Meta-Modeling Power Consumption Forecasting Approach Combining Client Similarity and Causality. *Energies* **2021**, *14*, 6088. [CrossRef]
28. Kim, Y.; Oh, H. Comparison between Multiple Regression Analysis, Polynomial Regression Analysis, and an Artificial Neural Network for Tensile Strength Prediction of BFRP and GFRP. *Materials* **2021**, *14*, 4861. [CrossRef]
29. Kalita, K.; Chakraborty, S.; Madhu, S.; Ramachandran, M.; Gao, X.-Z. Performance Analysis of Radial Basis Function Metamodels for Predictive Modelling of Laminated Composites. *Materials* **2021**, *14*, 3306. [CrossRef] [PubMed]
30. PIDOTECH Inc. *PIAnO User's Manuals and Tutorials*; PIDOTECH Inc.: Seoul, Korea, 2019.
31. Chung, S.-U.; Lee, J.-Y. Teeth Arrangement and Pole–Slot Combination Design for PMLSM Detent Force Reduction. *Energies* **2021**, *14*, 8141. [CrossRef]